C. R. Physique 13 (2012) 257–267

Contents lists available at SciVerse ScienceDirect

Comptes Rendus Physique

www.sciencedirect.com

Use of large scale facilities for research in metallurgy

Study of diffusive transformations by high energy X-ray diffraction

Étude des transformations diffusives par diffraction des rayons X à haute énergie

G. Geandier [a,*], E. Aeby-Gautier [a], A. Settefrati [a], M. Dehmas [a], B. Appolaire [b]

[a] *IJL/SI2M, UMR CNRS Nancy Université 7198, École des Mines, parc de Saurupt, 54042 Nancy, France*
[b] *LEM, ONERA/CNRS, 29, avenue Division Leclerc, BP 72, 92322 Châtillon cedex, France*

ARTICLE INFO

Article history:
Available online 28 January 2012

Keywords:
High energy X-rays
Diffraction
Microstructure
Phase transformations
Titanium alloys
Steels

Mots-clés :
Rayons X de haute énergie
Diffraction
Transformations de phase
Alliage de titane
Aciers

ABSTRACT

High energy X-ray diffraction is a powerful tool, able to follow phase transformations during complex thermal or thermo-mechanical treatments. High energy allows one to study volumic specimens of a few mm^3 and get successive data within a few seconds or less. The technique is described with different experimental setups (heating devices, detectors for diverse acquisition times) allowing diverse ranges for heating and cooling rates. Three examples are considered to illustrate the results obtained by using high energy X-ray diffraction. The first one corresponds to a simple diffusive phase transformation during an isothermal thermal path for the α–β transformation in a titanium alloy, highlighting the diffusive character considering the cell parameter evolutions of the parent phase. The second one illustrates the precipitation sequences observed during ageing of a β-metastable phase in a titanium alloy that was not obtained by TEM. The last example illustrates the phase evolutions during ageing of a martensitic steel showing the complexity of cell parameters evolution and some evolutions of the stress state.

RÉSUMÉ

La diffraction des rayons X de haute énergie est un outil puissant pour suivre les transformations de phases pendant des traitements thermiques ou thermo-mécaniques complexes. La haute énérgie permet d'étudier des échantillons massifs de plusieurs mm^3 et d'obtenir des données toutes les secondes ou moins. La technique est décrite avec différents dispositifs expérimentaux (fours, détecteurs pour différents temps d'acquisition) permettant une large gamme de vitesse de chauffage et de refroidissement. Trois exemples sont considérés pour illustrer les résultats obtenus en utilisant la diffraction des rayons X de haute énergie. Le premier correspond à une simple transformation de phases diffusive pendant un traitement thermique isotherme pour la transformation α–β dans un alliage de titane, mettant en lumière le caractère diffusif en considérant les évolutions des paramètres de mailles de la phase parente. Le second illustre les séquences de précipitation observées lors du vieilllisement d'une phase β métastable dans un alliage de titane qui n'a pu être obtenu par MET. Le dernier exemple illustre les évolutions de phases durant le vieillissement d'un acier martensitique montrant la complexité des évolutions des paramètres de mailles et quelques évolutions de l'état de contrainte.

* Corresponding author.
E-mail address: guillaume.geandier@ijl.nancy-universite.fr (G. Geandier).

1631-0705/$ – see front matter
doi:10.1016/j.crhy.2011.12.001

1. Introduction

In many cases, material properties are achieved after a sequence of treatments involving solid–solid phase transformations. Optimising these properties requires a deep understanding of: (i) the relationships between the processing parameters and the mechanisms involved in the microstructure formation and evolution; as well as (ii) the relationships between the resulting microstructures and the properties. Hence, it appears clear that investigating the mechanisms and predicting the kinetics are key steps to design and control microstructures with some desired properties. In order to monitor solid–solid phase transformations, a large number of characterisation techniques are available such as X-ray or neutron diffraction, optical and electronic microscopies. Most often, the kinetics of rapid phase transformations are inferred from the measurement of some relevant physical property: length for transformations exhibiting volume changes, magnetic or electrical properties associated with the transformation, etc. X-rays diffraction is less commonly used for obtaining kinetics of phase transformations. Indeed, it remains mainly a basic technique to characterise the crystallographic structures of all phases present. However, it is worth noting that quantitative analyses of the diffraction patterns give the lattice parameters as well as the volume fraction of each phase. Thus, laboratory equipment can be used to follow the phase evolutions based on these parameters in variable conditions involving temperature or stresses. However, in order to determine them accurately, acquisition times must be quite long. This limits the investigations with such equipment to very slow kinetics. Moreover, as a consequence of the small depth penetration of laboratory X-rays in metallic materials, the analysed volume is located near the surface. Any surface reactivity with environment will thus interfere with the other observed phenomena and must be limited, if not controlled. The limitations of the laboratory equipment can be largely overcome using synchrotron radiation at high energy (about 90 keV and over). First, large volumes can be analysed by transmission of X-rays through millimetre wide samples. Second, acquisition times are drastically reduced to a few seconds or less. Hence, coupled with heating devices, high energy X-rays permit to collect a large series of Debye–Scherrer diffraction diagrams during controlled thermal or thermo-mechanical solicitations: the nature of the phases, the lattice parameters of their structures and their volume fractions can be accurately determined versus time to monitor the transformations in the bulk of materials. Moreover, it must be stressed that additional information concerning the evolution of average strain or composition can be retrieved from the full width at half maximum of the diffraction peaks.

Due to all these advantages and with the growing number of high energy facilities, this technique has become more and more popular these last years (see e.g. [1–14]). For our part, we have benefited from the European Synchrotron Radiation Facility (ESRF) to investigate phase transformation in different alloys, such as titanium alloys, aluminium alloys or steels. In the present article, we will first discuss some technical and methodological issues of this technique. Then we will illustrate its potentialities by focusing on a simple case, the isothermal phase transformation after cooling from the high temperature range in a titanium alloy and on more complex behaviour, i.e. during ageing of two specific industrial alloys: (i) the precipitation sequences observed during ageing of a β-metastable titanium alloy; and (ii) the simultaneous evolutions of several phases during ageing of a martensitic steel.

2. Experimental methods

Phase transformation studies using X-ray diffraction require a good spatial resolution for the diagrams, a temporal resolution to follow phase evolutions during thermal treatments as well as a good statistic on the diffracting domains. In the case of high energy experiments [15], spatial resolution is given by the detector type (number and size of pixels) and the set-up geometry; namely the distance between the sample and the detector, the size of the detector. Time resolution is dependent on the type of detector and the choice of the time resolution is dependent on the kinetics of the phase transformation studied. The counting statistics on the phases are given by: (i) the high energy synchrotron beam which allows analysing a large volume (here several mm^3) [16]; (ii) the rotation of the sample if grain size is particularly large; and (iii) the detector that allows recording data over a large solid angle [17–19].

High energy diffraction (≈ 90 keV) was used to follow the phase transformations during thermal treatments in steels [4,20], aluminium alloys [5], and titanium alloys [9,11,12]. The structural changes were characterised during continuous heating or cooling and during isothermal treatments. For all following examples, high energy diffraction was used to study a large volume of the sample. Experimental results are thus representative of the bulk material and minimise the surface effects. In such conditions, complex sample environments (inert gas or vacuum chamber) can be removed as the surface effects are very low compared to the volume (estimated at 1 or 2%). However, surface effects may affect the obtained results in some specific cases.

2.1. Set-up for thermal experiments

Different set-up were used, that were specially devoted to the phase transformation kinetics considered. Resistance furnaces that are suitable to slow kinetics, allow maximum heating/cooling ramps of 10 °C/min. For slow kinetics, the use of a fast detector is not mandatory; so the choice can be an image plate detector, as a MAR345 [21]. This detector has a long readout time (around 2 min) but a very good spatial resolution at high angle due to the technology used to read the plate: a laser reads the signal and erases the plate following a spiral trajectory, meaning a huge number of pixels at high angle. Radiant furnaces allow more rapid heating and cooling rates (up to about 10 °C/s). They are thus more adapted to

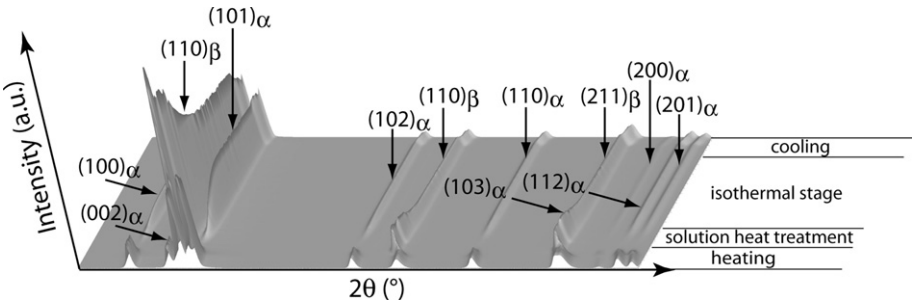

Fig. 1. Diffraction diagrams evolution over time for a β-metastable titanium alloy (Ti17).

study kinetics in isothermal conditions (after rapid heating or cooling). For rapid temperature variations as well as rapid transformation kinetics, fast 2D CCD (Charge-Coupled-Device) detectors are generally used (MARCCD [21], FReLoN [22], Pixium [23]), in order to record diagrams every 1–3 seconds. All furnaces can be driven controlling the temperature with a thermocouple welded or not on the sample, or controlling the electric power supplied to the furnace. During our treatments, in some cases, samples were placed in continuous rotation in order to increase the number of diffracting grains. In this case, power driving method was used to control the temperature variations.

High energy diffraction is made using a synchrotron beam with an energy around 89 keV ($\lambda = 0.0139$ nm) in the case of the ID15B beamline. Higher energy can be reached at the ESRF on ID11 or ID15A and on other synchrotron sources (Diamond, DESY, APS, Spring8, etc.). The detector is placed at a distance between 0.6 and 1.2 meters, depending on its geometry. Generally, the 2θ range usable is 0–10°.

2.2. Set-up calibration

The experimental set-up being a flexible part on a synchrotron beamline, it is necessary to calibrate all parts for each experiment. In order to follow precisely the phase evolutions, we need to know with a high precision the wavelength, the distance between the sample and the detection plan and the non-orthogonality of the detector according to the beam. To determine these parameters, we used standard powders with known structure and cell parameters (CeO_2, LaB_6, ...). Powders were placed at the sample position, and diffraction diagrams were recorded at different positions of the detector. We used at least two positions for the detector in order to calibrate the distance and the wavelength. The non-orthogonality of the detector was deduced from the refinement of the powder diffraction rings. Data reduction was proceeded using software as fit2d [24] to correct and to integrate the 2D images to classical 1D diffractograms usable for further analysis.

2.3. Data analysis

To study the phase transformation, 2D images were fully reduced to 1D diffractogram in order to limit the effect of grainy rings, texture reinforcement and the low number of grains in the diffracting volume. Fig. 1 shows successive diffractograms obtained during thermal treatment of a titanium alloy (heating, dwell, cooling, isothermal dwell and final cooling). The evolutions of peaks intensities highlight the domains of phase evolutions.

Diagrams were analysed using a Rietveld's approach [25]. The method was developed for neutron study and adapted later for X-rays. Due to the large volume of data, we used software that is suitable for making automatic treatment, as Fullprof [26]. The first step of the analysis was to determine a set of parameters that fit the experimental data and then make the calculations for the following data. As phase evolutions were considered, special attention was paid when the phase fraction became very small. From this analysis realised for each diagram, extracted results were: phase amounts (mass fractions in general), cell parameters, Full Width at Half Maximum (FWHM), background, etc.

3. Results

In situ studies of phase transformations by HEXRD lead to characterisation of the nature of the phases, the transformation kinetics and the cell parameters of each phase. The involved structural changes and the variations of phase fractions are basic data to study phase transformations kinetics. In numerous diffusive transformations, the formation of the new phase is associated with a partitioning of solute elements between the parent phase and the product phase. The modification of chemical composition of the parent and product phases and in consequence the modification of their cell parameter, is thus a good indicator of a diffusion process. However, considering a solid–solid phase transformation, it is also necessary to be sensitive to the existence of stresses associated with the transformation strains and to the differences in Coefficient of Thermal Expansion (CTE). Those stresses may also influence the evolution of cell parameter of the phases.

In order to illustrate results that can be obtained by HEXRD, we present at first a simple case of phase transformation during cooling in isothermal condition of a titanium alloy, in which the expected transformation is obtained. In a second step we consider the transformation during ageing of a supersaturated β-metastable phase obtained after solution treatment

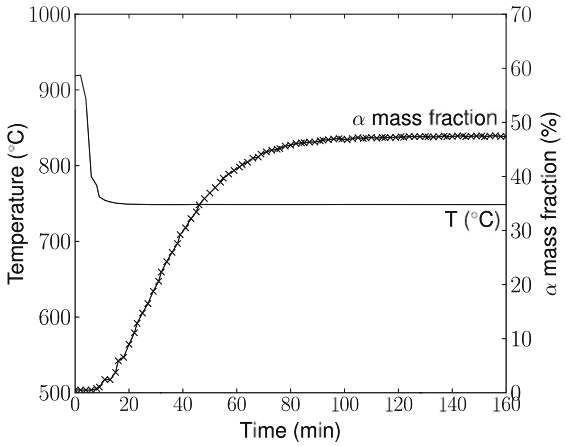

Fig. 2. Variations of temperature and α mass fraction versus time during cooling and isothermal holding (Ti17 alloy).

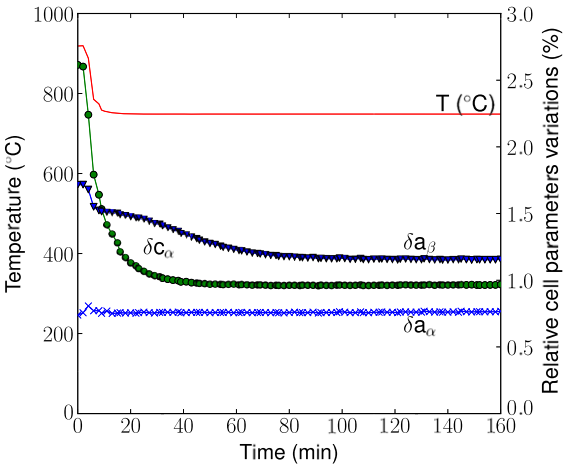

Fig. 3. Variations of temperature and relative cell parameters versus time during cooling and isothermal holding (Ti17 alloy).

in the single β temperature range and cooling and in a third one the transformation during ageing in a martensitic stainless steel.

3.1. Isothermal transformation in a β-metastable titanium alloy [11,12]

Titanium presents an allotropic transformation at 882 °C from the high temperature β phase (BCC) to the α phase (HCP). Addition of alloying elements may result in a two phase domain ($\alpha + \beta$) at a temperature lower than the β transition temperature. The $\beta \rightarrow \alpha + \beta$ transformation has been studied in isothermal conditions using HEXRD for Ti17 alloy. The composition is in mass%: Al 5, Mo 4, Cr 4, Zr 2, Sn 2. Its β transition temperature is 880 °C. After a solution treatment at 920 °C in the β temperature range, the specimen is cooled to the transformation temperature and maintained at that temperature.

If we focus on the successive diffraction diagrams recorded during the isothermal holding in Fig. 1, the appearance of the peaks characteristic of the α phase are clearly observed as well as their increase in intensity. Moreover, a continuous change of the β peak's position can be noticed. The quantitative analysis of the diffraction diagrams led to the evolution of phase amount (Fig. 2) and to the relative variations of the cell parameters (Fig. 3) during the cooling and isothermal holding steps.

The α mass fraction which is close to zero at the beginning of the holding step, increases following an S-shape evolution. The maximal amount formed at about 750 °C is of 47%. It can be mentioned that the obtained kinetics are similar to those obtained by electrical resistivity [12,27].

The relative cell parameter is defined as $\delta a_\phi = (a_\phi(t) - a_\phi(0))/a_\phi(0)$ for cell parameter a of phase ϕ; $a_\phi(0)$ is the cell parameter of phase ϕ, at 20 °C, at the beginning of the experiment. A constant value of the relative cell parameter indicates that the cell parameter remains constant in the range considered.

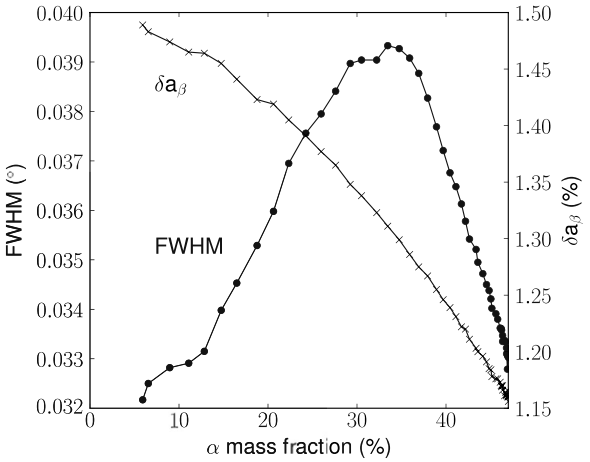

Fig. 4. Variations of relative cell parameters of β phase and $(200)_\beta$ FWHM versus α mass fraction (Ti17 alloy).

Considering the parent phase, a first decrease in δa_β is observed associated with the cooling step. As the temperature remains nearly constant, δa_β does not decrease anymore until the mass fraction of α increases. Within the transformation range, a continuous decrease of δa_β is observed and this parameter does not vary any more once the transformation is completed. These variations may be correlated to the change in chemical composition of β. For the α phase, δa_α remains constant as transformation proceeds, except at the very beginning of the transformation, as temperature decreases (the amount of α is of about 3%). However, a strong decrease of δc_α is observed during cooling, as α mass fraction increases from 0.5% to 2.5%. A smoother decrease is observed until $t = 30$ min, corresponding to an α mass fraction of 30 min and the beginning of the transformation.

For the case considered, the changes in cell parameter during the holding step are associated with changes in the chemical composition of the phases. Indeed, one can expect a quite small contribution of the elastic deformation of the phases since the flow stress of the beta phase is low (about 60 MPa at a deformation rate of 3×10^{-4} s^{-1} [28]). The cell parameter variations of beta phase are thus associated with changes in its chemical composition as shown by Héricher and Dehmas for Ti17 alloy [29,30]. A further correlation between δa_β and α mass fraction is reported in Fig. 4; in addition the variations of FWHM of $(200)_\beta$ peak are reported.

The α formation leads to a decrease of δa_β and at the same time the FWHM increases until a mass fraction reaches 33% and decreases again. A similar behaviour was observed for isothermal transformation at 700 °C and 600 °C. The amplitude of the isothermal decrease of δa_β increases as the α mass fraction formed increases. This is related to the increasing differences in composition between the parent β phase and the remaining one. The quantitative estimation of those changes was realised by Bruneseaux [12] considering the chemical composition of the β phase measured in the alloy by Héricher [29] and cell parameters variations with composition using a Vegard's law. The increase of FWHM can easily be understood taking into account the morphology of the α precipitates which consists mainly in colonies with α lamellae and enriched β phase. The colonies grow from the β/β grain boundaries in the parent grain of which composition is less modified. The difference in composition between the parent β phase and the enriched one leads to an increase of FWHM. When transformation tends to be completed, the chemical composition of β tends to a homogeneous one and FWHM decreases.

The large variations of δc_α are mainly attributed to changes in the mean composition of interstitial elements in the α phase and namely in oxygen. Indeed, the cell parameters of α have been shown to strongly depend on the oxygen content [2]. Our experiments were realised in air, allowing a diffusion of oxygen. In consequence, the surface layers enriched in oxygen will favour the formation of α (a small amount is formed on cooling to 750 °C) with a mean composition in oxygen larger than that of the α phase formed in the bulk. At the first minutes of transformation we mainly analyse the α phase in the surface layers. When the overall fraction of α increases, the mean value of δc_α decreases and reaches a constant value when α mass fraction is larger than 25%.

3.2. Transformation during ageing in β-metastable titanium alloys [31]

Mechanical properties of β-metastable titanium alloys can be increased by forming precipitates during ageing. After a solution treatment in the β temperature range, a rapid cooling to room temperature leads to a β-metastable phase, i.e. a supersaturated β solution. A further ageing leads to the decomposition of the parent β-metastable phase.

Heat treatment parameters, such as heating rate, ageing temperature or chemical composition of the β-metastable phase may influence the transformation process. This is clearly illustrated in Fig. 5 giving SEM micrographs of specimens of Ti-5553 alloy (nominal composition in wt% Ti–5Al–5Mo–5V–3Cr) aged at 650 °C for three different heating rates which contain a same amount of α and β phases. Depending on the heating rate, the α precipitates (in dark contrast on the micrographs) present large differences in size and morphology. The lower the heating rate, the finer the microstructure. For the lower

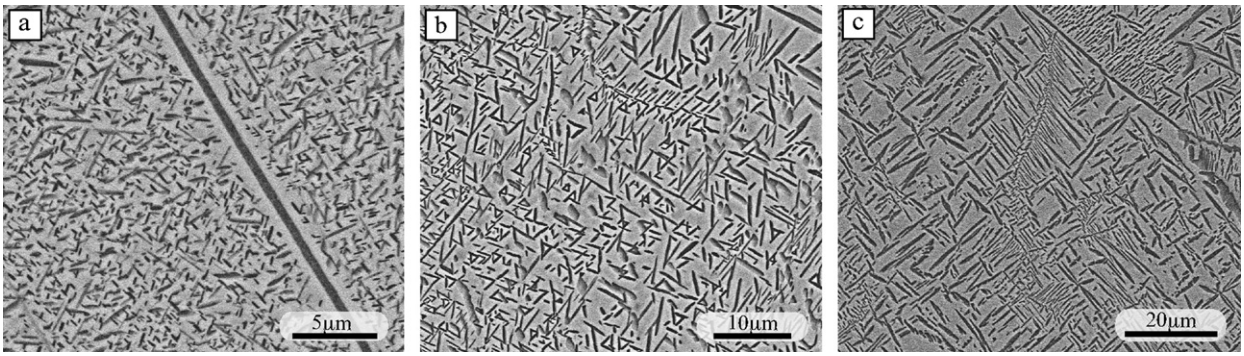

Fig. 5. SEM micrographs obtained after ageing two hours at 675 °C for three different heating rates of about (a) 0.1 °C/s; (b) 1 °C/s; (c) 3 °C/s (Ti-5553 alloy).

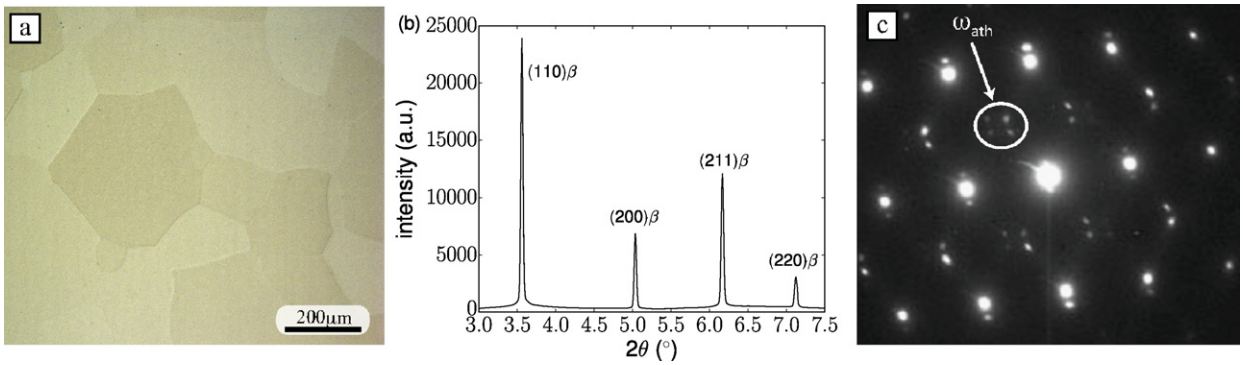

Fig. 6. (a) Optical micrograph of β-solutionized and quenched Ti-5553 sample; (b) X-ray diffraction pattern of the as-quenched structure; (c) Selected-area diffraction pattern of $\langle 110 \rangle \beta$ zone axis showing additional reflections associated with ω_{ath} precipitates.

heating rate (0.1 °C/s) very small quasi-equiaxed precipitates are obtained, distributed homogeneously in the β grain. Precipitation along the grain boundary can be noticed too, surrounded by a precipitate free zone. For a heating rate near to 1 °C/s, acicular precipitates are obtained with a well defined orientation. At the higher heating rate (3 °C/s), coarse and elongated α precipitates are observed, with both inter and intragranular precipitation.

Different authors have studied the precipitation process during ageing of β-metastable phase in different β-metastable alloys. The formation of a metastable hexagonal isothermal ω (ω_{iso}) phase is often reported, followed by the formation of the hexagonal α phase [32–35]. The ω_{iso} precipitates are generally considered as nucleation sites for the α precipitates. A few authors studied the influence of the heating rate on the precipitation process using either in situ electrical measurements or XRD and TEM analysis on specimens quenched at different temperatures during heating. It was shown that electrical resistivity variations differ depending on the heating conditions, indicating changes in the transformation temperature ranges. The change in electrical resistivity could be associated with structural changes thanks to TEM observations that evidenced formation of ω_{iso} and α. Only few analyses by XRD relate the formation of orthorhombic α'' before the formation of α phase [36,9,37,33].

In situ HEXRD experiments were thus performed to analyse the precipitation sequences. At first, samples were solution treated at 890 °C for 30 min, temperature above the β transition temperature (847 °C for our Ti-5553 alloy). After solution treatment, samples were rapidly cooled to room temperature by switching off the furnace, so the cooling rate was around 100 °C per second at the beginning. In situ study of phase evolutions during the solution treatment and rapid cooling was performed. In the as-quenched condition, the Ti-5553 alloy exhibits a single-phase microstructure with large equiaxed β grains, as shown in Fig. 6. The XRD patterns recorded on cooling and at room temperature confirm that α precipitation does not occur (Fig. 6(b)). Moreover, they did not reveal any athermal ω (ω_{ath}) formation. However, the presence of ω_{ath} within the β grains was evidenced by TEM using electron diffraction (Fig. 6(c)).

The second step of the heat treatment consisted in ageing the samples at 650 °C for two hours using three different heating rates. Fig. 7 shows the evolution of $(I, 2\theta)$ diffraction patterns obtained during heating until 650 °C and 2 hours ageing at this temperature for the three different heating rates.

At the initial state, diffraction pattern reveals only peaks of the β phase. During heating at 0.1 °C/s (Fig. 7(a)), first changes are observed between 325 °C and 420 °C, except modifications in the β peak position due to the temperature increase. The formation of ω phase is evidenced with the appearance of two peaks at $2\theta = 5.7°$ and 6.7°. When the temperature exceeds 420 °C, peaks corresponding to ω_{iso} disappear and double peaks located at 5.5° and 6.55° appear. These peaks cannot be identified as the hexagonal α phase. They are characteristics of an orthorhombic structure, called α''. As

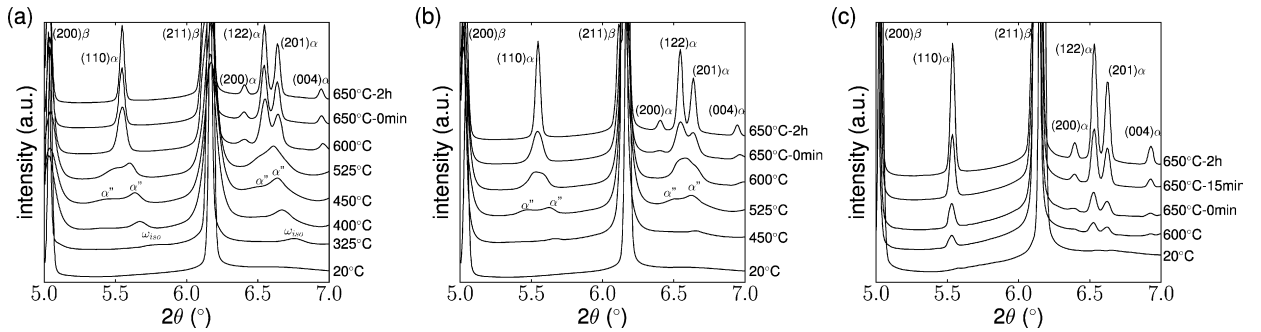

Fig. 7. Evolution of the diffraction patterns obtained: (i) during heating to 650 °C and during the isothermal step at this temperature for heating rates of about (a) 0.1 °C/s; (b) 1 °C/s; (c) 3 °C/s (Ti-5553 alloy).

the transformation proceeds, the intensity of α'' peak increases strongly between 420 °C and 540 °C, whereas that of β phase peak decreases. At 525 °C, the double peaks get nearer and they can longer be distinguished at temperatures above 540 °C. These peaks thin gradually and their centred position moves toward the final position of α peak showing that α'' disappears to the profit of α. When the specimen reaches 650 °C, only α and β peaks are observed on the diffraction patterns. During holding at this temperature, the intensity and the position of the peaks of both phases do not vary. Figs. 7(b) and 7(c) illustrate the evolution of the diffraction patterns using a heating rate of 1 °C/s and 3 °C/s, respectively. For those higher heating rates, the formation of ω_{iso} could not be evidenced anymore. At 1 °C/s, α'' peaks appear directly between 450 °C and 600 °C. At the higher heating rate (3 °C/s), the beginning of precipitation is evidenced at about 600 °C. The peaks characteristic of the α structure are clearly identified at temperatures above 610 °C.

The results obtained by HEXRD allow determining the precipitation sequence for this alloy, a sequence that depends on the heating rate. The lower heating rate favours the formation of ω_{iso}, as mentioned in the literature. As the temperature increases, the orthorhombic α'' appears and replaces ω_{iso}. Our results clearly evidence the formation of α'', rather than α as mentioned in the literature. The formation of α can only be evidenced at temperatures near 500 °C.

From the observed microstructure (Fig. 5), it can be expected that ω_{iso} acts as nucleation sites for α''. As temperature increases, a continuous change of α'' toward α is observed. This change can be associated with a more efficient diffusion of solute elements in order to tend to the equilibrium structure and composition of the α phase. Increasing the heating rate to 1 °C/s, does not allow the formation of ω_{iso}. The formation of α'' is, however, possible. After ageing it results in plates lying in (101) plans of the parent β grain. At last, the heating rate of 3 °C/s does not allow the formation of α''. We observe a direct transformation to the α phase.

The identified precipitation sequences are similar to those observed during ageing the 100% β-metastable phase in the metastable titanium alloy Ti17 [11]. The comparison between the two alloys shows that the precipitation kinetics are dependant on the chemical composition of the alloy. This results was confirmed by additional studies on precipitation during ageing on Ti-5553 alloy with a matrix enriched in β stabilising elements. Increasing the amount of β stabilising elements in the supersaturated matrix leads to a slower kinetics of ω_{iso} and α'' formation.

3.3. Transformation on ageing of a high nitrogen martensitic stainless steel [20,38]

In martensitic steel, different phase transformations occur during the heating of the as-quenched structure: the transformation from martensite to ferrite and that from retained austenite to ferrite, both with rejection of alloying elements and formation of precipitates. In the case of Fe–C–N steel alloyed with Cr, Mo and V, a complex competition opposes carbon and nitrogen atoms in their redistribution during the low-temperature ageing and in the formation of precipitates at higher tempering temperatures [39]. The in situ X-ray diffraction gave the opportunity to obtain simultaneously the evolution of all phases, as long as they were detectable by XRD.

The steel studied (X40CrMoVN16-2-EN1.41123-S42.025-AMS 5925) was provided by Aubert & Duval with the following composition in wt%: 0.40 C, 0.20 N, 0.28 V, 1.7 Mo, 15.6 Cr, Fe bal. In the annealed state, the microstructure consisted in a mixture of ferrite and precipitates. Those are $(Fe,Cr,Mo)_{23}C_6$ carbides and hexagonal primary $(Cr,V)_2N$ nitrides. The samples were first submitted to a solution treatment at 1050 °C during 45 min, followed by air quenching to room temperature. The as-quenched matrix was composed of martensite and retained austenite. The mass fraction of retained austenite, determined by HEXRD, was about 26%. Primary precipitates, present in the annealed state, were not totally dissolved during the solution treatment [4]. The as-quenched microstructure still contained precipitates with mass fractions of about 2% of undissolved primary fcc $(Fe,Cr,Mo)_{23}C_6$ carbides and 0.5% of undissolved primary hexagonal $(Cr,V)_2N$ nitrides. The specimens were further heated up to several temperatures at a heating rate of 12 °C/min. In the following we present results obtained for a specimen heated to 800 °C.

Fig. 8(a) presents the succession of 44 diffraction diagrams illustrating the evolution of (111) residual austenite and (101) martensite diffraction peaks on heating from room temperature to 800 °C, for 2θ ranging from 3.80° to 4.05°. Fig. 8(b)

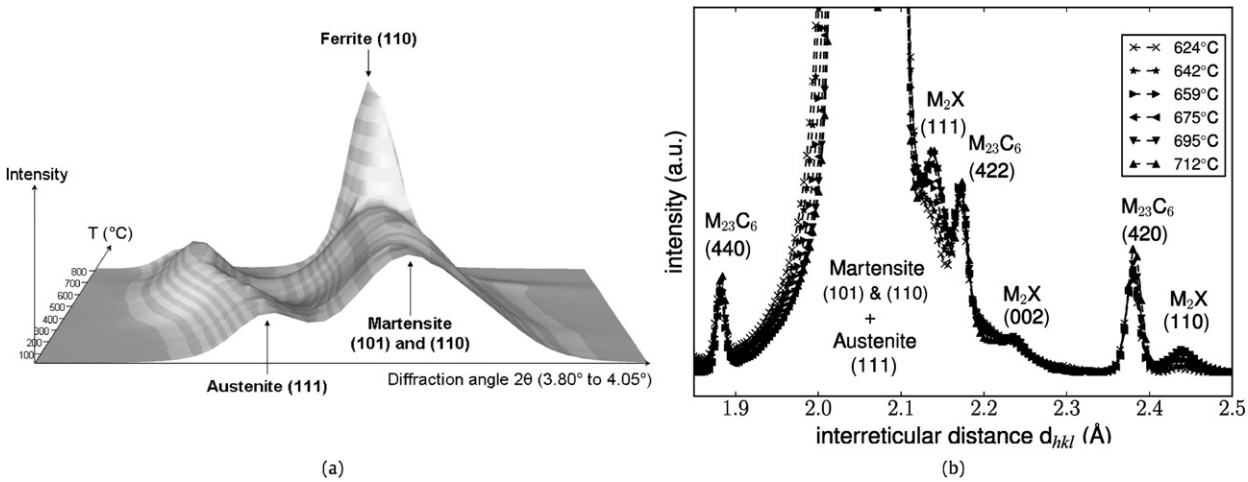

Fig. 8. (a) Evolution of (111) residual austenite and (101) and (110) martensite diffraction peaks on heating from room temperature to 800 °C. (b) Diffraction diagrams recorded at several temperatures on heating for interreticular distances d ranging from 1.85 Å and 2.50 Å.

Table 1
Lattice parameters of the structures in as-quenched state.

Structures	Lattice parameters (nm)
Martensite	a 0.28699 ± 0.00004
	c 0.29181 ± 0.00007
Retained austenite	a 0.35986 ± 0.00003
$M_{23}C_6$	a 1.0637 ± 0.0006

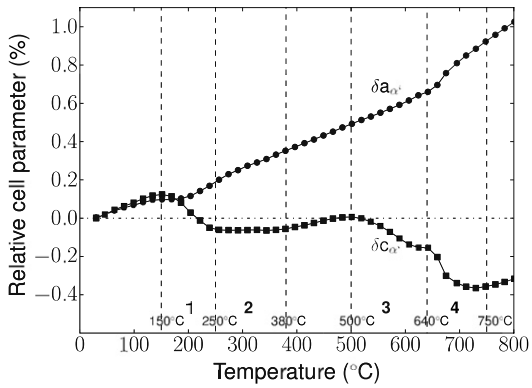

Fig. 9. Evolution of relative variations of martensite lattice parameters versus temperature.

represents 6 successive diffraction diagrams between 624 °C and 712 °C highlighting the evolutions of several reflections of $M_{23}C_6$ and M_2X structures.

The crystallographic structures detected during the heating up to 800 °C were the same as in the as-quenched state: martensite/ferrite, austenite, fcc $M_{23}C_6$ and hexagonal M_2X. However we observed changes in the amount of phases and their cell parameters.

The relative in situ evolutions of the martensite lattice parameters $\delta a_{\alpha'}$ and $\delta c_{\alpha'}$ as a function of the temperature are plotted in Fig. 9. In each case, the as-quenched state measured at the beginning of the experiment is taken as the reference. The cell parameter at room temperature are given in Table 1.

The results obtained show a nonlinear behaviour in the relative cell parameter variations. As for the evolution of $\delta a_{\alpha'}$ and $\delta c_{\alpha'}$, the thermal dilatation alone would promote an increase of both lattice parameters with a derivative coefficient close to the dilatation coefficient of the ferrite (about 11×10^{-6} K^{-1} in this steel). Here, the nonlinear evolutions of $\delta a_{\alpha'}$ and above all $\delta c_{\alpha'}$ indicate the transformation of the martensite into ferrite. Below 150 °C, the evolutions of $\delta a_{\alpha'}$ and $\delta c_{\alpha'}$ were similar, with a derivative coefficient close to the dilatation coefficient of the ferrite. Above 150 °C, the parameter $a_{\alpha'}$ always increased, with minor variations of the derivative coefficient while the parameter $c_{\alpha'}$ underwent two contraction stages: the one at low temperatures (150–380 °C) and the other at high temperatures (500–750 °C). The temperature range 150–380 °C

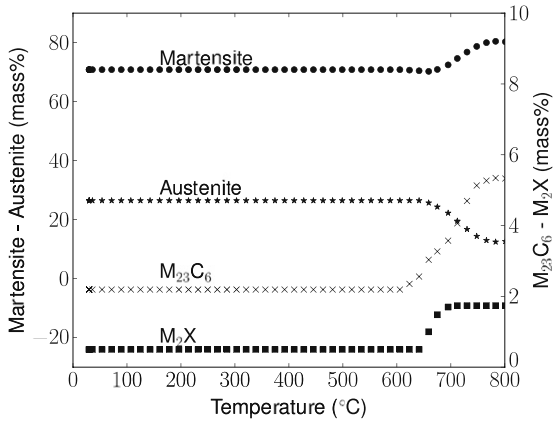

Fig. 10. Evolution of mass fractions of the phases (martensite, retained austenite, $M_{23}C_6$ and M_2X) as a function of the temperature up to 800 °C.

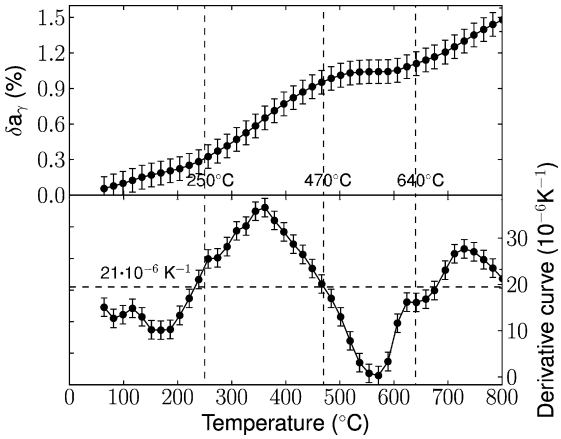

Fig. 11. Variations of the relative cell parameter of retained austenite and its derivative as a function of the temperature up to 800 °C.

was divided into two parts: a strong decrease (stage 1) followed by a slow decrease (stage 2). The temperature range 500–750 °C was also divided into two parts (stage 3 and stage 4). To the fourth stage corresponds a marked acceleration of the increase of $a_{\alpha'}$. In addition, the Full Width at Half Maximum (FWHM) of the martensite diffraction peaks strongly decreased at about 650 °C (see Fig. 8(a)).

The linked evolutions of $a_{\alpha'}$ and $c_{\alpha'}$ were a result of the transformation from the tetragonal martensitic structure into the cubic ferritic structure, with a rejection of alloying elements, in particular C and N. Indeed, a strong decrease of $c_{\alpha'}$ and a low increase of $a_{\alpha'}$ with decreasing the fraction of dissolved C (or N) in Fe–C (or Fe–N) as-quenched martensites was reported by numerous authors and reviewed by L. Cheng et al. [40]. Carbon and nitrogen occupy octahedral interstices of the martensitic tetragonal lattice and their rejection out of the martensite affects the lattice parameters in such a way: the two first-nearest-neighbour metallic atoms along the c axis are brought closer one from another in the direction of the empty interstice (decrease of $c_{\alpha'}$) and the four second-nearest-neighbour metallic atoms are slightly pushed away in the plane perpendicular to the c axis (increase of $a_{\alpha'}$) [40]. In our case, we could identify four successive decreasing periods of $c_{\alpha'}$, corresponding to four successive precipitation stages in the martensite. The corresponding increase of $a_{\alpha'}$ is evident for the fourth stage. Quantitative analysis of $c_{\alpha'}/a_{\alpha'}$ were done in [20], associating those variations with the amount of interstitial solute rejected from the tetragonal martensite.

The evolution of the mass fraction of all phases (martensite/ferrite, retained austenite, $M_{23}C_6$ and M_2X) is reported in Fig. 10. The decrease in austenite amount is observed at temperatures above 640 °C. The mass fraction of $M_{23}C_6$ carbides started to increase at 550 °C, slightly during the third stage of martensite decomposition, and more continuously between 600 °C and 800 °C. In this last temperature range, an increase of the M_2X mass fraction is also observed, much more rapid than that of $M_{23}C_6$. These more rapid evolutions are also illustrated in Fig. 8(b). At last, variations of a/c ratio of M_2X were also evidenced, associated with changes in their chemical composition [20,38].

The relative in situ evolution of the austenite lattice parameter δa_γ and the derivative curves as a function of the temperature are plotted in Fig. 11. The austenite lattice parameter δa_γ increases with the temperature, but the derivative coefficients shows important variations. The measured derivative coefficients are compared to the coefficient of thermal expansion (CTE), equal to 21×10^{-6} K^{-1} and measured in the fully austenitic structure before the transformation from

austenite to martensite during quenching. Comparing the derivative coefficients of Fig. 11 to austenite CTE, four steps are delimited. Up to about 250 °C, the retained austenite derivative coefficient is lower than austenite CTE and equals approximately 15×10^{-6} K^{-1}. Between 250 °C and 450 °C, the derivative coefficient is higher than austenite CTE, with a maximum of 37×10^{-6} K^{-1}. In the temperature range 450–650 °C, the derivative coefficient is lower than austenite CTE, with a minimum of 1×10^{-6} K^{-1}. In the high temperature range corresponding to the decrease of the retained austenite fraction (650–800 °C), the derivative coefficient varied between 17×10^{-6} K^{-1} and 28×10^{-6} K^{-1}. Deviations of the derivative coefficient from austenite CTE during the heating are caused by chemical or mechanical evolutions. Up to 250 °C, a chemical evolution of the structure is excluded. The low value of the derivative coefficient of a_γ is thus ascribed to additional elastic strains. Indeed, in the mixed retained austenite/martensite structure the difference in CTE between austenite and martensite leads to stresses. A micromechanical evaluation of these stresses leads to compression stresses in the residual austenite and in consequence to a cell parameter lower than the expected one considering only temperature variations. Between 250 °C and 450 °C, the high derivative coefficient of a_γ is associated with a stress relaxation of the austenitic structure, consecutive to the beginning of the transformation from martensite to ferrite. The increase in the austenite cell parameter due to composition changes is not expected. At those temperatures, it is mainly C which diffuses and only an increase in carbon would lead to an increase in the austenite cell parameter. An increase in carbon amount is not expected (i.e. the formation of transition carbides occurs in the martensite laths, or at their interfaces). However, the change in the c/a ratio leads to a volume decrease of the martensite which modifies the stress states in the phases. In the present case, the mean stress which is expected to be in compression after martensitic transformation [41] increases leading to an positive elastic mean strain variation. In the temperature range 450–700 °C, the low derivative coefficient of δa_γ is ascribed to a chemical evolution of the non-equilibrium retained austenite. The rejection of alloying elements toward the poorer composition of the ferrite caused the diminution of the lattice parameter. This chemical evolution started about 200 °C under the beginning temperature of the austenite to ferrite transformation. During the transformation from austenite to ferrite (660–770 °C), the derivative coefficient was close to the reference derivative coefficient of the austenite.

A quantitative analysis of all these variations needs to develop a complex model combining the microstructural evolutions and their consequence on the stress free cell parameters and a micromechanical model.

4. Conclusion

High energy X-ray diffraction is a powerful tool for structural evolution studies associated with solid–solid phase transformations. Data are obtained in real time and are representative of the bulk behaviour. Multiple experimental devices can be used to apply controlled complex thermal or thermo-mechanical treatments on specimen. A large range of heating and cooling rates can be studied due the available furnaces and detectors type. 2D detectors permits to collect large solid angle of the diffraction signal with a high precision and adaptable frame rates. Synchrotron beam allows to quantify small amount of phase (less than 1%) with a high level of precision.

Quantitative characterisation of a large volume of data can be made by Rietveld's analysis to extract phase fraction evolutions over time and temperature as well as their cell parameter variations. Depending on the phase transformation, obtained results can highlight the transformation mechanisms involved (diffusive with chemical changes). Following the cell parameter and the FWHM of diffraction peaks allows one to extract data about the changes in the chemical composition, or in the stress states in each phases.

These points have been illustrated during the studies of phase transformation during the isothermal $\beta \rightarrow \alpha + \beta$ transformation on cooling of a titanium alloy, as well as during the ageing of a β-metastable phase in a titanium alloy and the ageing of martensite in a martensitic stainless steel. The high quality of the results obtained by this technique, the simultaneous in situ evolutions of all obtained data allow going further in the analysis of the transformation mechanism involved and give new insights in the micromechanical approaches of solid–solid phase transformations. Evolution of the stress state of phase during phase transformation is a new field of research that is accessible with the high energy X-ray diffraction. Moreover, the quantitative results obtained can be further used to validate the microstructure evolution models.

References

[1] S. Offerman, N.V. Dijk, J. Sietsma, S. Grigull, E. Lauridsen, L. Margulies, H. Poulsen, M. Rekveldt, S.V.D. Zwaag, Grain nucleation and growth during phase transformations, Science 298 (2002) 1003–1005.
[2] S. Malinov, W. Sha, Z. Guo, C. Tang, A. Long, Synchrotron X-ray diffraction study of the phase transformations in titanium alloys, Materials Characterization 48 (2002) 279–295.
[3] S. Babu, E. Specht, S. David, E. Karapetrova, P. Zschack, M. Peet, H. Bhadeshia, In-situ observations of lattice parameter fluctuations in austenite and transformation to bainite, Metallurgical and Materials Transactions A 36 (2005) 3281–3289.
[4] A. Bénéteau, P. Weisbecker, G. Geandier, E. Aeby-Gautier, B. Appolaire, Austenitization and precipitate dissolution in high nitrogen steels: an in situ high temperature X-ray synchrotron diffraction analysis using the Rietveld method, Materials Science and Engineering A 393 (2005) 63–70.
[5] M. Dehmas, P. Weisbecker, G. Geandier, P. Archambault, E. Aeby-Gautier, Experimental study of phase transformations in 3003 aluminium alloys during heating by in situ high energy X-ray synchrotron radiation, Journal of Alloys and Compounds 400 (2005) 116–124.
[6] J. Elmer, T. Palmer, S. Babu, E. Specht, In situ observations of lattice expansion and transformation rates of alpha and beta phases in Ti–6Al–4V, Materials Science and Engineering A 391 (2005) 104–113.
[7] B. Kaouache, K. Inal, S. Berveiller, A. Eberhardt, E. Patoor, Martensitic transformation criteria in Cu–Al–Be shape memory alloy – in situ analysis, Materials Science and Engineering A 438–440 (2006) 773–778.

[8] T. Ohba, T. Taniwaki, H. Miyamoto, K. Otsuka, K. Kato, In situ observations of martensitic transformations in Ti50Ni34Cu16 alloy by synchrotron radiation, Materials Science and Engineering A 438–440 (2006) 480–484.
[9] F. Bruneseaux, G. Geandier, E. Aeby-Gautier, M. Dehmas, P. Boulet, In situ characterization of the transformation sequences of Ti17 alloy by high energy X-ray diffraction. Influence of the thermal path, in: Ti-2007 Science and Technology, Proc. 11th Conference on Titanium JIMIC, vol. 5, 2007, pp. 565–566.
[10] E. Jimenez-Melero, N. van Dijk, L. Zhao, J. Sietsma, S. Offerman, J. Wright, S.V. der Zwaag, Martensitic transformation of individual grains in low-alloyed TRIP steels, Scripta Materialia 56 (2007) 421–424.
[11] F. Bruneseaux, E. Aeby-Gautier, G. Geandier, J.D.C. Teixeira, B. Appolaire, P. Weisbecker, A. Mauro, In situ characterizations of phase transformations kinetics in the Ti17 titanium alloy by electrical resistivity and high temperature synchrotron X-ray diffraction, Materials Science and Engineering A 476 (2008) 60–68.
[12] F. Bruneseaux, Apport de la diffraction des rayons X à haute énergie sur l'étude des transformations de phases. Application aux alliages de titane, PhD thesis, Institut National Polytechnique de Lorraine, 2008.
[13] B. Malard, Caractérisation multiéchelle par diffraction de neutrons et rayonnement synchrotron de la transformation martensitique sous contrainte dans un alliage à mémoire de forme CuAlBe, PhD thesis, École Nationale Supérieure d'Arts et Métiers, 2008.
[14] J. Hell, M. Dehmas, G. Geandier, N. Gey, S. Allain, A. Hazotte, J. Château, Influence of the austempering temperature on the microstructure and crystallography of a carbide-free bainitic steel, Solid State Phenomena 172–174 (2011) 797–802.
[15] T. Tschentscher, P. Suortti, Experiments with very high energy synchrotron radiation, Journal of Synchrotron Radiation 5 (1998) 286–292.
[16] P.J. Withers, Depth capabilities of neutron and synchrotron diffraction strain measurement instruments. I. The maximum feasible path length, Journal of Applied Crystallography 57 (2004) 596–606.
[17] H.F. Poulsen, S. Garbe, T. Lorentzen, D.J. Jensen, F.W. Poulsen, N.H. Andersen, T. Frello, R. Feidenhans'l, H. Graafsma, Applications of high-energy synchrotron radiation for structural studies of polycrystalline materials, Journal of Synchrotron Radiation 4 (1997) 147–154.
[18] O.V. Mishin, E.M. Lauridsen, N.C.K. Lassen, G. Bruckner, T. Tschentscher, B. Bay, D.J. Jensen, H. Poulsen, Application of high-energy synchrotron radiation for texture studies, Journal of Applied Crystallography 31 (1999) 364–371.
[19] K.-D. Liss, A. Bartels, A. Schreyer, H. Clemens, High-energy X-rays: a tool for advanced bulk investigations in materials science and physics, Textures and Microstructures 35 (2003) 219–252.
[20] A. Gurgey-Bénéteau, Étude des conditions de dissolution des carbures dans les aciers à roulement martensitiques à haute teneur en azote, PhD thesis, Institut National Polytechnique de Lorraine, 2007.
[21] MAR-research, Hamburg, http://www.rayonix.com/products/sx_165.htm, 2011.
[22] J.-C. Labiche, O. Mathon, S. Pascarelli, M.A. Newton, G.G. Ferre, C. Curfs, G. Vaughan, A. Homs, D.F. Carreiras, The fast readout low noise camera as a versatile X-ray detector for time resolved dispersive extended X-ray absorption fine structure and diffraction studies of dynamic problems in materials science, chemistry, and catalysis, Review of Scientific Instruments 78 (2007) 091301.
[23] J.E. Daniels, M. Drakopoulos, High-energy X-ray diffraction using the Pixium 4700 flat-panel detector, Journal of Synchrotron Radiation 16 (2009) 463–468.
[24] A.P. Hammersley, S.O. Svensson, A. Thompson, Calibration and correction of spatial distortions in 2D detector systems, Nuclear Instruments & Methods in Physics Research A 346 (1994) 312–321.
[25] H.M. Rietveld, A profile refinement method for nuclear and magnetic structures, Journal of Applied Crystallography 2 (1969) 65–71.
[26] J. Rodriguez-Carvajal, Recent advances in magnetic structure determination by neutron powder diffraction, Physica B 192 (1993) 55–69.
[27] E. Aeby-Gautier, F. Bruneseaux, J. Da-Costa-Teixeira, B. Appolaire, G. Geandier, S. Denis, Microstructural formation in Ti alloys: In-situ characterization of phase transformation kinetics, Journal of Materials (January 2007) 55–58.
[28] M. Khelifa, E. Aeby-Gautier, S. Denis, P. Archambault, J. Sarteaux, Analysis of the mechanical behaviour of metastable β titanium alloys. Influence of the phase transformation, in: G. Lütjering, J. Albrecht (Eds.), Ti-2003, Science and Technology, Proc. 10th Conference on Titanium, Wiley–VCH, 2003, pp. 1599–1606.
[29] L. Héricher, Prévision des microstructures lors du traitement thermique d'alliage de titane, PhD thesis, Institut National Polytechnique de Lorraine, 2004.
[30] M. Dehmas, J. Kovac, E. Aeby-Gautier, B. Appolaire, B. Denand, J. Da-Costa-Teixeira, $\beta \rightarrow \beta + \alpha$ isothermal phase transformation in Ti17 titanium alloy: chemical composition and crystallographic aspect, Solid State Phenomena 172–174 (2011) 396.
[31] A. Settefrati, E. Aeby-Gautier, M. Dehmas, G. Geandier, B. Appolaire, S. Audion, J. Delfosse, Precipitation in a near β titanium alloy on ageing: Influence of heating rate and chemical composition of the β-metastable phase, Solid State Phenomena (2011) 760–765.
[32] R. Sanguinetti, M. Zandona, A. Pianelli, E. Gautier, Décomposition de la phase β-metastable de l'alliage de titane β-cez au cours du chauffage et du recuit, Journal de Physique IV 4 (1994) 99–103.
[33] Y. Ohmori, T. Ogo, K. Nakai, S. Kobayashi, Effects of ω-phase precipitation on β, α, α'' transformations in a metastable β titanium alloy, Materials Science and Engineering A (2001) 182–188.
[34] F. Prima, P. Vermaut, G. Texier, D. Ansel, T. Gloriant, Evidence of α-nanophase heterogeneous nucleation from ω particles in a β-metastable Ti-based alloy by high-resolution electron microscopy, Scripta Materialia (2006) 645–648.
[35] S. Nag, R. Banerjee, R. Srinivasan, J. Hwang, M. Harper, H. Fraser, ω-assisted nucleation and growth of α precipitates in the Ti5Al5Mo5V3Cr0.5Fe β titanium alloy, Acta Materialia (2009) 2136–2147.
[36] O.M. Ivasishin, P.E. Markovsky, Yu.V. Matviychuk, S.L. Semiatin, Precipitation and recrystallization behavior of beta titanium alloys during continuous heat treatment, Metallurgical and Materials Transactions A 34 (1) (2003) 147–158.
[37] R. Sanguinetti, M. Zandona, A. Pianelli, E. Gautier, Decomposition of β-metastable phase in β-cez alloy during continuous heating, Journal de Physique IV 3 (1993) 527–531.
[38] A. Bénéteau, B. Appolaire, E. Aeby-Gautier, G. Geandier, P. Weisbecker, A. Reidjaimia, T. Ganne, In situ synchrotron X-ray analysis of the behaviour of a martensitic stainless steel during ageing, in: G.O., et al. (Eds.), ICOMAT-08, TMS, 2008, pp. 191–198.
[39] V. Gavriljuk, H. Berns, High Nitrogen Steels, Springer-Verlag, ISBN 3-540-66411-4, 1999.
[40] L. Cheng, A. Bottger, T.D. Keijser, E. Mittemeijer, Lattice parameters of ironcarbon and ironnitrogen martensites and austenite, Scripta Metallurgica et Materialia 24 (1990) 509–514.
[41] E. Aeby-Gautier, G. Geandier, M. Dehmas, F. Bruneseaux, A. Bénéteau, P. Weisbecker, B. Appolaire, S. Denis, Évolutions des microstructures à l'état solide dans des matériaux polycristallins. Apport de la DRX à haute énergie aux études de cinétique et au comportement des phases, in: P. Goudeau, R. Guinebretière (Eds.), Rayons X et Matière (RX2009), Hermès Science, Lavoisier, 2011 (Chapter 5), http://www.lavoisier.fr/livre/notice.asp?id=3LKWX3A23LKOWL.